Individual variation in brain microstructural-cognition relationships in aging

Raihaan Patel[a,b*], Clare E. Mackay[c,d], Michelle G. Jansen[e], Gabriel A. Devenyi[a,f], M. Clare O'Donoghue[c,d], Mika Kivimäki[g], Archana Singh-Manoux[g,h], Enikő Zsoldos[c,d], Klaus P. Ebmeier[c], M. Mallar Chakravarty[a,b,f,l*], Sana Suri[c,d,l*]

[*]Corresponding author, [l]Joint senior authorship

[a]Computational Brain Anatomy Laboratory, Cerebral Imaging Centre, Douglas Mental Health University Institute, Verdun, Québec H4H 1R3, Canada

[b]Department of Biological and Biomedical Engineering, McGill University, Montréal, Québec H3A 2B4, Canada

[c]Department of Psychiatry, Warneford Hospital, University of Oxford, OX3 7JX, Oxford, United Kingdom

[d]Oxford Centre for Human Brain Activity, Wellcome Centre for Integrative Neuroimaging, University of Oxford, OX3 7JX, Oxford, United Kingdom

[e]Donders Centre for Cognition, Donders Institute for Brain, Cognition and Behaviour, Radboud University, Nijmegen, the Netherlands

[f]Department of Psychiatry, McGill University, Montréal, Québec H3A 1A1, Canada

[g]Department of Epidemiology and Public Health, University College London, WC1E 6BT London, United Kingdom

[h] Université de Paris, Inserm U1153, Epidemiology of Ageing and Neurodegenerative diseases, 75010 20 Paris, France

Abstract

While all individuals are susceptible to age-related cognitive decline, significant inter- and intra-individual variability exists. However, the sources of this variation remain poorly understood. Here, we examined the association between 30-year trajectories of cognitive decline and multimodal indices of brain microstructure and morphology in older age. We used the Whitehall II Study, an extensively characterised cohort using 3T brain magnetic resonance images acquired at older age (mean age = 69.52 ± 4.9) and 5 repeated cognitive performance assessments between mid-life (mean age = 53.2 ±4.9 years) and late-life (mean age = 67.7 ±4.9). Using non-negative matrix factorization, we identified 10 brain microstructural components that integrate measures of cortical thickness, surface area, fractional anisotropy, and mean and radial diffusivities. We observed two modes of variance that describe the association between cognition and brain microstructure. The first describes variations in 5 microstructural components associated with low mid-life performance across multiple cognitive domains, decline in reasoning abilities, but a relative maintenance of lexical and semantic fluency from mid-to-late life. The second describes variations in 5 microstructural components that are associated with low mid-life performance in lexical fluency, semantic fluency and short-term memory performance, but a retention of abilities in multiple domains from mid-to-late life. The extent to which a subject loads onto a latent variables predicts their future cognitive performance 3.2 years later (mean age = 70.87 ±4.9). This data-driven approach highlights a complex pattern of brain-behavior relationships, wherein the same individuals express both decline *and* maintenance in function across cognitive domains and in brain structural features.

Significance Statement

Although declines in cognitive performance are an established aspect of aging, inter- and intra-individual variation exists. Nevertheless, the sources of this variation remain unclear. We analyse a unique sample to examine associations between 30-year trajectories of cognitive decline and multimodal indices of brain anatomy in older age. Using data-driven techniques, we find that age-related cognitive decline is not uniform. Instead, each individual expresses a mixture of maintenance and decline across cognitive domains, that are associated with a mixture of preservation and degeneration of brain structure. Further, we find the primary determinants of late-life cognitive performance are mid-life performance and higher brain surface area. These results suggest that early and mid-life preventative measures may be needed to reduce age-related cognitive decline.

1.0 Introduction

Cognitive decline is a well-established aspect of the aging process. Age-related impairments which impact everyday functioning have been reported across a range of cognitive domains (1, 2). However, significant inter-individual variability has also been observed across cognitive domains including memory, spatial functioning, processing speed and reasoning. While some individuals experience

accelerated rates of deterioration, others experience a relative maintenance of cognitive functioning into old age (3–5). Even within the same individual, some cognitive domains may remain intact whereas other domains are more vulnerable to decline (6). It is unclear whether this intra- and inter-individual variation arises from underlying changes already present in early-to-mid life, or if they are established in older age. Improving our understanding of the sources of this variability is an important step in understanding aging-related changes in cognition.

Numerous studies have used structural and diffusion magnetic resonance imaging (MRI) techniques to assess the structural substrates of brain aging. In particular, MRI provides macro- and microstructural measures such as volume, thickness, surface area, diffusivity and fractional anisotropy, each of which convey complementary information about the local morphology, axonal density, organization and myelination of the cerebral cortex (7, 8). In healthy aging, these techniques have demonstrated widespread age-related degeneration of brain structure via decreases in overall brain volume (9), cortical thickness (10–12), and fractional anisotropy as well as increases in diffusivity (7, 13–15). Further to this, the reserve hypothesis suggests differences in brain structure, be it through differences in neurobiological capital at a given time (brain reserve) or in development of age-related brain changes over time (brain maintenance), may partially explain variation in cognitive function (16). This proposed brain-cognition link in aging individuals has been supported by various studies, for example by previously established associations between episodic memory performance with volumes and diffusivity of the medial temporal lobe (17–20), and between decline in executive functioning and widespread grey matter atrophy (18). However, most studies to date have considered these micro- and macro-structural MRI metrics individually, without considering the complementary information multiple metrics provide on brain structure, or their potential overlap and interdependencies.

This study builds on previous analyses in two important ways. We integrate multiple MRI based indices of cortical microstructure, and explore individual differences in brain-cognition relationships without *a priori* designations of cognitive trajectories. Incorporating data from multiple MRI modalities is useful as each conveys complementary information, such that the resulting multimodal assessments query a wider range of biological phenomena (7). This approach has enabled fine grained assessments of the cerebral cortex. Glasser et al., for example, incorporated data from structural and functional MRI to delineate a novel parcellation of the cortex, including the identification of de novo areas distinguishable as a result of this strategy (21). Seidlitz et al. integrated multimodal MRI indices of cortical microstructure to identify morphometric networks, such that areas of the cortex displaying morphometric similarity shared cytoarchitectonic and transcriptional features (22). These findings demonstrate the specificity of associations demonstrated using multimodal MRI. Here, we leverage multivariate techniques and multimodal MRI to investigate patterns of covariance and their relationship to cognition. By modelling shared covariance across MRI metrics, as opposed to separately analysing each piece of information, this allows for a more comprehensive assessment of differences across subjects (23). To this end, we use non-negative matrix factorization (NMF), a matrix decomposition technique previously used in our group to probe microstructural properties of the hippocampus (24). Applied to MRI data, NMF highlights regions of the brain in which shared patterns of microstructural variation occur, as well as subject-specific measurements describing individual microstructural features within the highlighted brain regions. (24–26).

Previous approaches investigating brain-cognition relationships have defined subject groupings based on cognitive trajectories and then assessed group differences in brain structure (18, 27). For example, individuals have been categorised as cognitive "maintainers", or "decliners" (28). A common strategy is to categorize the most severe decliners and compare them to the rest of a cohort (18). This approach usually involves arbitrary cut-offs, and may be biased by the extremes of the decline-maintain dimension, neglecting individuals demonstrating neither sharp decline nor strong maintenance (29). Furthermore, broad categorisations of maintainers/decliners may also ignore intra-individual heterogeneity and the differential impact of age across cognitive domains (30–32).

In this study, we analyse data from the Whitehall II cohort. This ongoing study was established in 1985 at University College London and initially included 10,308 British civil servants (33). Longitudinal follow-up occurred at multiple timepoints (defined throughout as Waves) roughly every five years at Wave 5 (1997-1999), 7 (2002-2004), 9 (2007-2009), 11 (2012-2013), and 12 (2015-2016). At each Wave, information on social, cognitive, and biological data was collected, resulting in a unique source of information to study aging. Eight hundred individuals from Wave 11 were randomly selected to participate in the Whitehall II Imaging sub-study (Imaging Wave, 2012-16) in which structural, diffusion, and functional MRI was collected (34). In this work, we integrate the longitudinal cognitive assessments and MRI data to study relationships between late life cortical microstructure and cognitive performance trajectories from mid to late life.

2.0 Results

Using the comprehensive lifespan data from the Whitehall II Imaging sub-study, we analyse longitudinal cognitive trajectories across multiple domains and assess their relationship with late-life cortical microstructure using surface area (SA), cortical thickness (CT), mean diffusivity (MD), fractional anisotropy (FA) and radial diffusivity (RD). Across multiple microstructural MRI indices, we model shared covariance using NMF, and employ mixed effects modeling to extract person specific indices of baseline performance and change in performance across multiple cognitive tests. We then use partial least squares (PLS), a multivariate technique capable of identifying patterns of covariance between microstructure and longitudinal cognitive performance (35, 36). Finally, we use each individual's expression of the identified patterns to predict cognitive function at a follow-up timepoint, approximately 3.2 years after the MRI scan (Wave 12) (Figure 1).

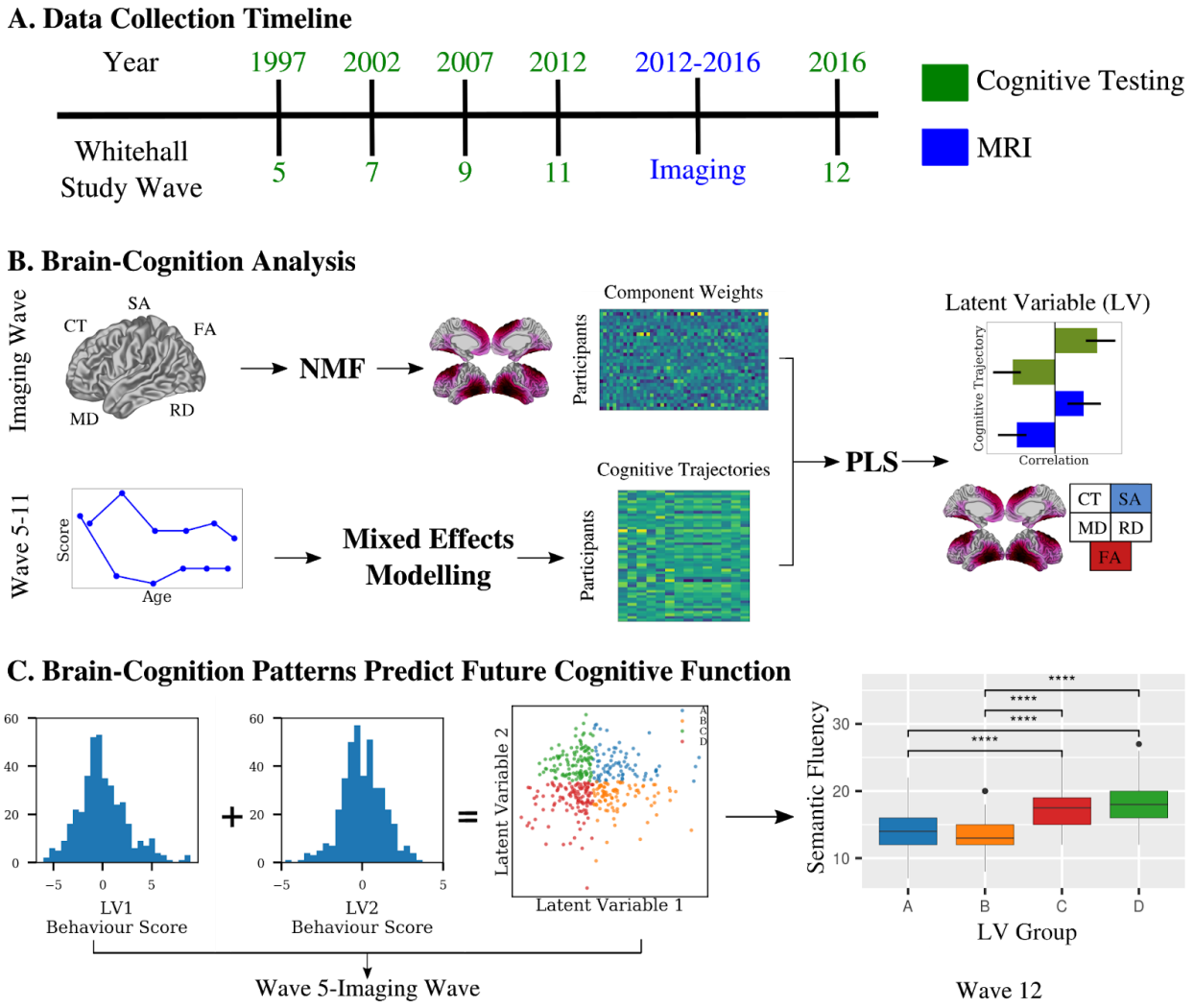

Figure 1. **Identifying microstructural-cognition relationships in aging using data-driven techniques.** A) We analysed data from the Whitehall II Imaging Sub-Study. Participants were tested across multiple cognitive domains at ~5-year intervals since 1997, with structural and diffusion MRI collected between Waves 11 and 12. B) We applied non-negative matrix factorization (NMF) to five metrics of cortical morphology: cortical thickness (CT), surface area (SA), fractional anisotropy (FA), and mean and radial diffusivity (MD, RD) to identify patterns of variance. Using cognitive data from Wave 5-11, we applied mixed effects modelling to identify baseline and slope measurements for each individual across a range of cognitive tests. We then used a partial least squares (PLS) analysis to identify latent variables describing covarying patterns between longitudinal cognitive trajectories and late life cortical morphology. C) We grouped participants based on their expression of brain-cognition relationships, and these groupings were indicative of future cognitive performance at Wave 12.

2.1 Sample

The final analysis sample included 398 individuals who passed quality control for motion and cortical thickness processing, and had whole brain DWI available (mean age = 69.5 years ± 4.2, 92 females (23%), mean education years = 14.2 ± 3). Comparison of the analysis and initial samples is shown in Table 1. For further details on sample selection, see SI Methods and Figure S1.

Table 1: Demographic characteristics for the analysis and starting samples including mean and standard deviations for age, years of education, and MOCA score at the MRI Phase. Number of women, as well as number of individuals with MOCA score >=26, indicative of no major cognitive impairments, is shown as well. Statistical tests (t-test or chi-squared) show no differences between the analysis sample and full starting sample.

	Analysis sample (N=398)	**Starting sample (N=775)**	**Test Statistic**	***p***
Age (years)	69.52 ± 4.9	69.81 ± 5.19	$t = 0.95$	0.35
Education (years)	15.84 ± 3.54	15.72 ± 3.53	$t = -0.58$	0.57
MOCA score	27.29 ± 2.23	27.18 ± 2.26	$t = -0.80$	0.42
Women, N (%)	92 (23.1%)	150 (19.3%)	chi-squared = 2.27	0.13
MOCA>=26, N (%)	322 (80.9%)	614 (79.2%)	chi-squared = 0.46	0.49
N (%) of participants scanned on Verio MRI scanner	281 (70.6%)	552 (71.2%)	chi-squared = 0.49	0.82

2.2 Non-negative matrix factorization identifies 10 stable microstructural components

Each subject's T1-weighted image was processed using the CIVET algorithm (37, 38) to obtain measurements of CT and SA at each of 77122 vertices across the mid-surface (located halfway between inner and outer grey matter boundaries) mesh. Diffusion weighted imaging derived maps of FA, MD, and RD were co-registered to the T1-weighted image to allow for mid-surface sampling of these metrics. For each of the five microstructural metrics a 77122 x 398 (number of vertices x number of subjects) matrix was constructed, each of which was then concatenated to build a 77122 x 1990 (number of vertices x (number of subjects*5) multimodal input matrix which was input to NMF (24, 26). NMF is a decomposition technique which identifies spatial components and subject weightings, together identifying regions of the brain where microstructural variation is observed (spatial components) as well as each individual's microstructural profile in a given component (subject weightings). Together, these outputs localize individual variability to specific brain regions in a data-driven manner.

Split half stability analysis (24) identified 10 components as a suitable balance between spatial stability and reconstruction error (see SI Methods and Figure S2). The 10 spatial components and associated weightings are displayed in Fig 2. Each component identifies a group of vertices which share a covariance pattern for CT, SA, MD, FA, and RD. The components are largely bilateral and non-overlapping, and their regional descriptions and naming conventions are described below.

1. Component 1: (Fronto-Temporal) is localized in the superior frontal and posterior temporal regions.
2. Component 2: (Motor) is localized to primary and supplementary motor cortices, with some spread to adjacent posterior frontal and superior parietal regions.
3. Component 3: (Visual) is strongly localized in the medial and lateral occipital lobe, as well as the cingulate cortex and inferior temporal lobe.
4. Component 4: (Parietal) occupies most of the parietal cortex, with some spread to the lateral temporal regions.
5. Component 5: (Inferior Frontal) is most prominent in the inferior, medial frontal lobe, but also shows some presence in the inferior temporal lobe, anterior cingulate regions, and inferior lateral frontal lobe.
6. Component 6: (Anterior Frontal) occupies the anterior frontal regions as well as the temporal pole.
7. Component 7: (Cingulate) occupies much of the midline regions but with a strong preference to the cingulate cortex and shows some spread to insular cortices.
8. Component 8: (Postcentral) is heavily localized to the postcentral gyrus but shows considerable presence in the lateral inferior frontal lobe and superior temporal gyrus.
9. Component 9: (Right lateralized) is the only component showing a laterality effect, including bilateral medial parietal anterior temporal regions, but most prominent in right superior temporal and lateral inferior frontal regions.
10. Component 10: (Temporal Pole) is most prominent in the temporal pole, but also shows some presence in medial temporal and ventromedial frontal areas.

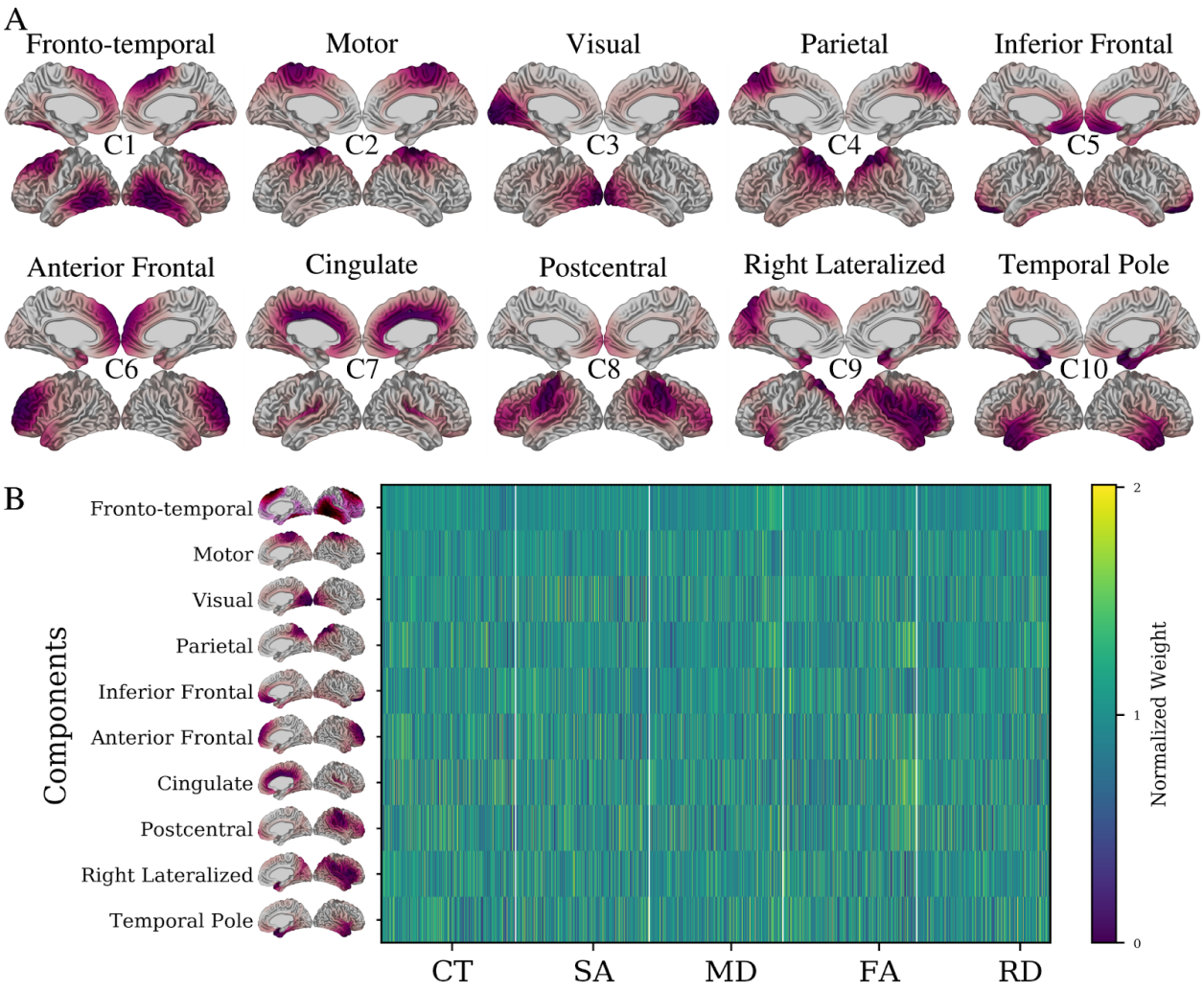

Figure 2. **10 microstructural components derived from the NMF decomposition.** A) Cortical mappings of each of the spatial patterns for each of the 10 components. For each component, lateral and medial views of both left and right hemispheres are shown. Components are identified using the putative descriptors from the main text (e.g., Fronto-temporal) as well as lettering at the centre of each set of surface views (e.g., C1). Red areas indicate vertices loading heavily onto a particular component (thresholded at 25% to max value). Each component identifies a selection of vertices sharing a microstructural variance pattern. Together, components cover the entire brain, are largely bilateral (with exception of component 9) and are not spatially overlapping. B) Subject-specific weightings associated with each of the displayed 10 components. Each row corresponds to a specific component's NMF weightings for each subject-metric combination, describing the CT, SA, MD, FA and RD patterns of each subject in each component. Together these two outputs describe the morphological patterns of each subject within each spatial component. Each element of the matrix is displayed as a fraction of its row mean, such that values below 0 indicate a below average weight for a given component and vice versa.

2.3 Specific Patterns of Cortical Morphology Relate to Baseline and Longitudinal Cognitive Function

We next related the variation in cortical microstructure captured by the NMF subject weightings to variability in cognitive performance over time. For each participant we derived the intercept and slope for the change in performance across each of seven cognitive tests: lexical and semantic fluency, short-term memory, verbal, mathematical and inductive reasoning, and vocabulary *(described in Methods)*. The intercept describes the estimated baseline (i.e., mid-life) performance while the slope describes the linear rate of change in performance over time (i.e., from mid-life to late-life). We then performed a brain-cognition PLS with NMF component weightings as "brain" data and intercept and slope measurements as "cognition" data. PLS is a multivariate technique which identifies latent variables describing covarying relationships between two sets of data (35, 36, 39), and here captures distributed brain-cognition patterns. PLS analysis identified two significant latent variables (LVs), explaining 57.1% and 20% of shared brain-cognitive covariance respectively. Each LV identifies a distinct pattern of longitudinal cognitive trajectories across the 30-year follow up that relate to patterns of late-life microstructural characteristics (Figure 3).

LV1 describes a pattern in which low baseline performance across all tests, accelerated 30-year decline in inductive, verbal, and mathematical reasoning abilities, but slow 30-year decline in verbal and semantic fluency are associated with global decreases in late-life SA, lower CT (cingulate/insular), lower FA (visual, temporal, right lateral), higher MD and RD (temporal pole), and paradoxically higher FA in posterior temporal and superior frontal regions. (Figure 3A, Table 2). LV2 describes a pattern in which low baseline performance in each of lexical fluency, semantic fluency, and short term memory, but slower decline in each of lexical fluency, semantic fluency, inductive reasoning, verbal reasoning, and numeric reasoning is associated with global increases in SA, higher CT and lower RD in the temporal pole, increased MD and RD in motor, anterior frontal, and cingulate cortices, and decreased FA (anterior frontal, cingulate/insular) (Figure 3B, Table 2).

In summary, we observed a mixed distribution for cognitive decline and maintenance, as well as degeneration and preservation of cortical microstructure. This mixed pattern suggests, rather than cognitive decline being linked with uniform cortical degeneration, that individuals display degrees of degeneration *and* preservation of cortical microstructure that is linked with decline *and* maintenance across diverse cognitive functions..

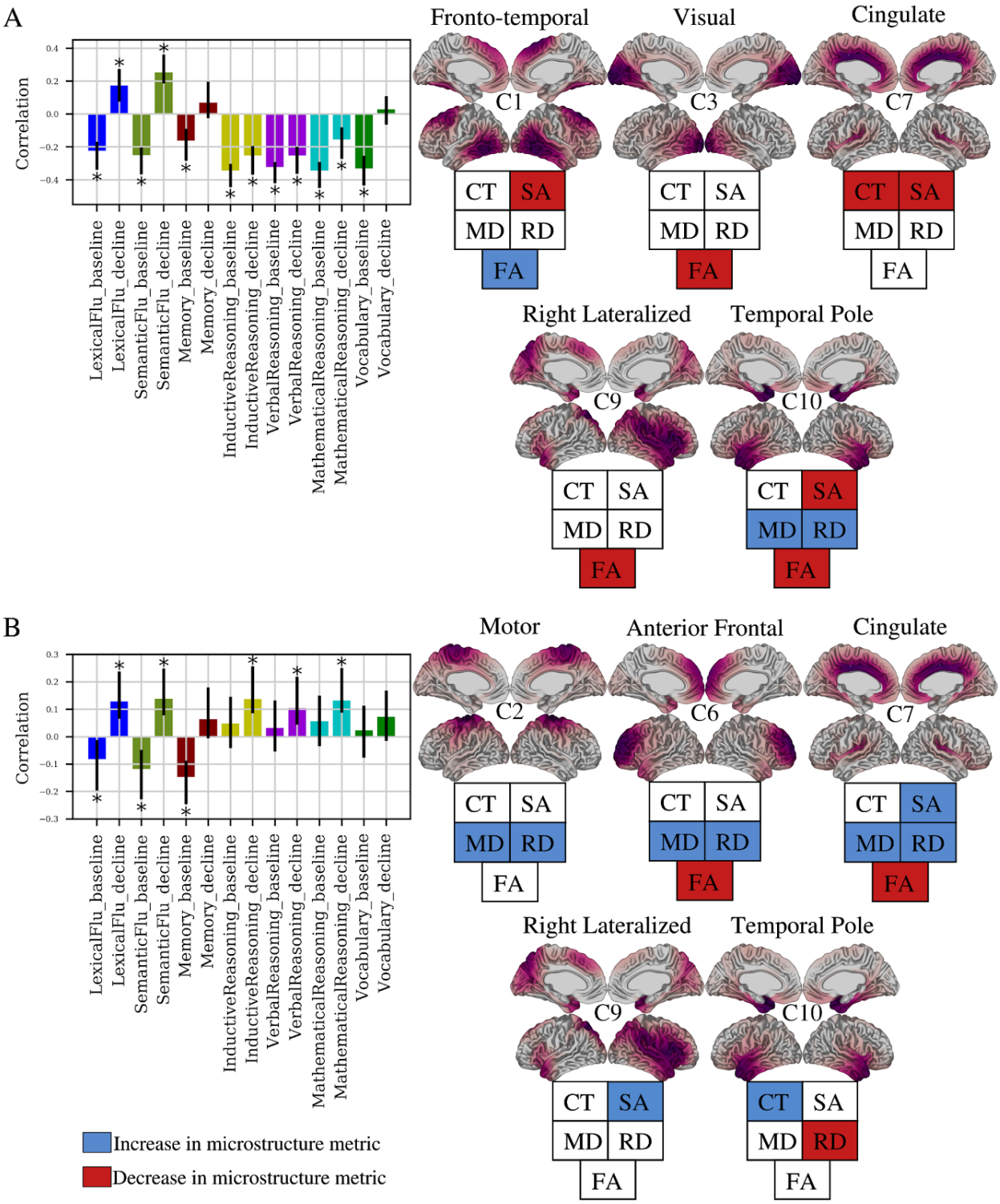

Figure 3: **Two brain-cognition latent variables identified by PLS**. PLS analysis identified two (LV1: A, LV2: B) significant latent variables ($p<0.05$), each identifying a pattern of correlation between NMF weightings, and cognitive intercept and slopes. Bar plots describe contribution of cognitive intercepts and slopes. The y-axis denotes correlation of each cognitive variable within a given LV. Error bars denote the 95% confidence interval, only variables with a non-zero confidence interval are described as contributing to a given LV (marked with *). For each

bar plot, cortical maps (right) show the spatial patterns of the components contributing to the LV. The fingerprint of each map describes whether a given metric is identified as being decreased (blue) or increased (red) in the spatial component in relation to the cognitive pattern shown in bar plots.

Table 2: Correlations of the contributing cognitive variables to each latent variable, including the mixed effects modelling parameter (intercept or slope), cognitive test, R and its 95% confidence interval (CI).

Latent Variable	Parameter	Cognitive Test	R [95% CI]
1	Intercept	Lexical Fluency	-0.22 [-0.34 , -0.17]
		Semantic Fluency	-0.25 [-0.37 , -0.2]
		Short Term Memory	-0.16 [-0.28 , -0.09]
		Inductive Reasoning	-0.34 [-0.44 , -0.3]
		Verbal Reasoning	-0.32 [-0.42 , -0.29]
		Mathematical Reasoning	-0.34 [-0.45 , -0.29]
		Vocabulary	-0.33 [-0.43 , -0.25]
	Slope	Lexical Fluency	0.17 [0.07 , 0.27]
		Semantic Fluency	0.25 [0.19 , 0.36]
		Inductive Reasoning	-0.25 [-0.37 , -0.19]
		Verbal Reasoning	-0.25 [-0.36 , -0.2]
		Mathematical Reasoning	-0.15 [-0.27 , -0.08]
2	Intercept	Lexical Fluency	-0.08 [-0.2 , -0.01]
		Semantic Fluency	-0.12 [-0.23 , -0.05]
		Short Term Memory	-0.15 [-0.25 , -0.09]
	Slope	Lexical Fluency	0.13 [0.07 , 0.24]
		Semantic Fluency	0.14 [0.08 , 0.25]
		Inductive Reasoning	0.14 [0.09 , 0.26]

		Verbal Reasoning	0.1 [0.04 , 0.22]
		Mathematical Reasoning	0.13 [0.09 , 0.25]

2.4 Brain-Cognition Patterns Predict Cognitive Performance at Future Timepoint

To further investigate the subject-level variation in the microstructural-cognition relationships identified by the two significant LVs, we stratified individuals into four groups based on the degree to which they expressed each LV. We then assessed how these groupings predicted cognitive performance at a future time point (Wave 12, 2015-16, on average 3.2 years post MRI collection). Within each LV, a behavior score was computed for each subject. For example, a subject with a positive LV1 behavior score would express the LV1 cognitive phenotype, whereas a subject with a negative LV1 behavior score would express the inverse cognitive pattern (Figure 4A). We plotted LV1 vs LV2 behaviors scores for each subject and created groupings within each quadrant such that the four groups (A-D) represent all pairwise positive/negative LV1/LV2 combinations (Figure 4B).

Groups A and B had a significantly higher proportion of cognitively impaired individuals (defined as MoCA < 26 at the time of the MRI scan) than Groups C and D (chi-squared = 35.359, $p < 0.01$, Figure 4C). Groups differed in terms of sex and education, but not age (SI Results and Figure S3). We next performed linear models, covarying for age, sex and years of education to examine if subject groupings differed in future cognitive performance at Wave 12. Across tests of semantic fluency, lexical fluency, and short-term memory, groups A and B (positive LV1) performed significantly worse than groups C and D (negative LV1). On tests of reasoning, groups A and B again performed significantly worse than groups C and D, but group C (negative LV1, positive LV2) outperformed group D (negative LV1, negative LV2) (Figure 4C).

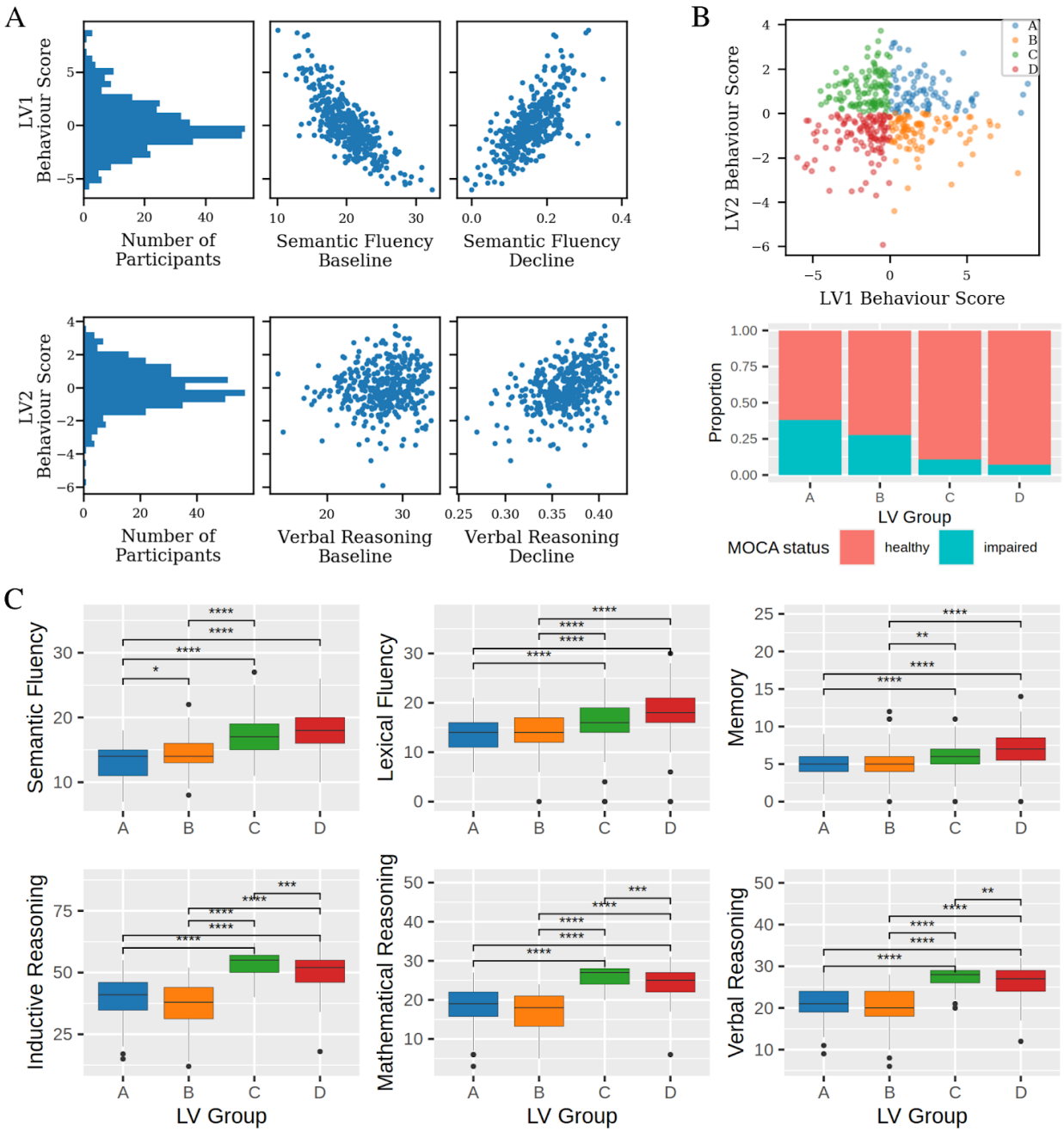

Figure 4: **Individual expression of PLS derived brain-cognition phenotype is indicative of cognitive status and future performance**. We used each subject's expression of LV1 and LV2 to predict their cognitive performance at a future wave (Wave 12, 3.2 years post Imaging Wave, on average). A) An illustration of the utility of LV behavior scores. Top row: a histogram shows the distribution of LV1 behavior scores, which quantify the degree to which each subject expresses the phenotype described by LV1. Plots of LV1 versus semantic fluency baseline and decline measures show positive and negative relationships, respectively. These match that described in LV1 in Figure 3, demonstrating that LV behavior scores can be used to describe the cognitive phenotype of subjects. Bottom row: equivalent plots for LV2 including the histogram, and plots of LV2 behavior scores vs verbal reasoning baseline (no relation) and verbal reasoning decline (positive relation). B) A plot of LV1 vs. LV2 behavior score for each

individual. Using this data, we defined four groups as each pairwise combination of positive/negative LV1/LV2. These groups differed significantly in terms of MOCA status (chi-squared = 35.359, $p<0.01$). C) This data driven group assignment is predictive of future cognitive performance. Each box plot shows the wave 12 cognitive performance of each of the four LV groupings. Colours correspond to the groupings in B. Main effect of LV Group was significant in each of the 6 tests at a bonferroni threshold of $p < 0.0083$ (0.05/6), and pairwise comparisons were assessed using Tukey's.

3.0 Discussion

In this study, we used a data-driven approach to identify microstructural-cognition patterns of covariance linking individual variation in cognitive decline over a period of 30-years from mid-to-late life, with later-life patterns of cortical microstructure. We integrated multimodal MRI data to fully capitalize on the complementary information conveyed by these indices of cortical microstructure. Importantly, we assessed this brain-cognition association without defining groups of maintainers or decliners beforehand, so as not to obscure intra-individual variation in cognitive ageing. We identified two significant latent variables describing patterns of covariance between longitudinal cognitive performance and cortical microstructure. Notably, these patterns did not reveal a homogenous or directionally uniform link between cognitive decline and degeneration of cortical microstructure. Instead we observed a more complex pattern whereby individuals presented a mixed distribution of 30-year cognitive decline *and* maintenance which were associated with both degeneration *and* preservation of cortical microstructure in older age. Finally, we found that the primary determinant of late-life cognitive performance was mid-life cognitive performance and an associated microstructural pattern dominated by cortical surface area.

3.1 Brain-Cognition relationships include a mixture of maintenance and decline

The brain-cognition relationships identified in this work contain a mixture of positive and negative features across both brain and cognition. LV1 describes a pattern of low midlife performance across all tests, accelerated decline in reasoning, but relatively maintained fluency associated with a multimodal pattern of low SA in all areas of the brain except for the primary and supplementary motor cortices, decreased CT in cingulate and insular cortex, increased diffusivity in the temporal pole, decreased FA in visual, temporal, and right lateral cortex but increased FA in superior frontal and lateral temporal regions. Meanwhile, LV2 links low baseline fluency and memory performance, but slower fluency and reasoning declines with increased diffusivities in nearly all regions except occipital cortex, increased surface area in cingulate, insular and right lateral areas, increased temporal pole thickness, and decreased FA in frontal, cingulate and insular regions. Thus, across both brain and cognition, we observe that each pattern includes a mix of what studies have traditionally characterised as adaptive and maladaptive characteristics. While it may be tempting to infer patterns of overall cognitive or neuroanatomical maintenance, our work suggests that by refraining from a priori definitions of maintenance or decline groups, including baseline and decline measures across a range of tests, and analysing multimodal indices of cortical microstructure simultaneously, we can identify subtle, complex brain-cognition relationships which show a mix of maintenance and decline features across both cognitive and anatomical measures. These findings thus

discourage the use of a 'one size fits all' approach, and instead encourage the consideration of cognitive domains and regional, multivariate anatomy at the individual level.

Ascertaining the neurobiological underpinnings of the MRI derived features of LV1 and LV2 remains challenging. Histological evidence links CT reductions in old age with decreased dendritic arborization (40, 41). A recent application of virtual histology supports this, having found cortical thinning is related to increased expression of CA1 pyramidal cell gene sets enriched with processes related to dendritic arborization approach correlated longitudinal CT changes with cell type expression levels (42, 43). Corresponding studies of SA remain uninvestigated, though see our discussion in Section 3.2 for more on our SA findings. DWI metrics may relate to a range of age-related alterations as decline in small diameter myelinated fibers, alterations in the myelin sheath, and inflammatory processes (13, 44). Increased diffusivity is a common finding in aging studies, and may relate to enlarged interstitial spaces or axon swelling (45–47). Rodent studies incorporating imaging and histology demonstrate that demyelination of axons leads to increased RD (48–51), while reductions in FA relate to degradation of structure and preferential orientation of fibers (48, 52). Thus we may hypothesize that LV1 has a neurobiological pattern of widespread reductions in cortical area, dendritic branching, demyelination, and axonal degeneration while LV2 is associated with near global demyelination and axonal degeneration, but relatively maintained cortical area in cingulate, insular, right lateral cortex and dendritic morphology in the temporal pole. However, while plausible, these interpretations are complicated by the fact that each MRI metric is sensitive to a large range of cellular level alterations (7, 53) as well as the interrelated nature of the DWI metrics analysed (45). While joint analyses of all metrics, as is a focus of this work, may help alleviate some concerns (54), caution is still warranted in absence of direct histological evidence.

3.2 Late Life Cognitive Performance is Driven by Mid Life Phenotypes

In our study sample and within the timeframe examined, the strongest predictor of later life (>65 years) cognitive performance across a range of tests was performance in midlife (at mean age of 40 years). Individuals scoring high on LV1 performed relatively worse across all cognitive domains in later life than those who expressed the inverse behavioral pattern. When stratifying subjects by their expression of both LV1 and LV2, a subset of individuals showed slower declines in reasoning and fluency, in addition to low midlife performance. However again, we found that the low midlife performance dominated late life performance on all tests, and better maintenance over time was not enough to compensate for a poor start. This finding has relevance to the concept of cognitive reserve. High levels of cognitive reserve, often probed through proxies such as education or occupational attainment, have been strongly linked to better cognitive function in aging (55). Whether this is driven by a maintenance of previously developed advantages, moderation of the effects of aging on cognition and hence cognitive decline, or a combination however remains unclear (55, 56). Our findings altogether suggest that midlife differences in cognitive performance were the most prominent predictors. However, it may be that individuals in our study sample have not yet reached a point of drastically accelerated decline and therefore showed relatively less profound differences in cognitive trajectories (57).

While the MRI data is cross sectional and collected only in late life, in the context of mid life dominance we find the widespread involvement of SA to be of particular interest. SA is commonly assessed in parallel with CT, though the contribution of each to cortical volume, as well as their neurobiological and genetic underpinnings (58–61), varies. For example, while each of SA, CT, and cortical volume decrease with age, CT and volume change are positively correlated while changes between CT and SA tend to be inversely related (60). SA decreases during aging are also of smaller magnitude than those observed for CT (60), and the primary determinant of SA, cortical column generation, occurs during prenatal and perinatal periods (58, 59). These findings suggest SA may be more temporally fixed than CT between mid and late life, and throughout the full lifespan. In this context, the pronounced influence of LV1 mid life cognitive performance and late life SA on late life cognition lends credence to a lifespan perspective in which developmental and mid-life events play a significant role in cognitive health in late life. In a unique study involving the Lothian Birth Cohort, positive cognitive ageing between childhood (age 11) and late life (age 73) was associated with higher SA in late life (62). In another unique study involving multiple samples, Walhovd et al. identified a large region of the cortex in which increased general cognitive ability was associated with increased surface area in a developmental sample (aged 4-12) and noted that this association persisted throughout the lifespan (63). Our findings, along with others, support the idea that stable advantages may give certain individuals a 'head start' in terms of cognitive function in aging. They also support the need for early and mid-life preventative measures of cognitive decline to maintain cognitive performance in older ages, though the potential role of reserve mechanisms on cognitive decline warrant further investigation. The mixed, complex relationships identified also support the development of individualized preventative strategies. Interestingly, within a subset of the Whitehall II cohort, previous work has identified similar mid to late life relationships across different biological domains such that midlife cardiovascular health was predictive of indicative of cerebral hypoperfusion in late life (64).

3.3 Strengths and Limitations

A key strength of this study is the use of multimodal MRI data to characterize cortical morphology. Use of multiple MRI metrics provides complementary information regarding anatomical properties of the brain in comparison to unimodal analyses. We take this further by employing NMF to analyse multimodal data simultaneously to capture shared patterns of covariance across measures. This approach allows us to identify 10 major components which are spatially contiguous and highlight relevant regions in which cortical morphology varies across subjects. We relate this variability to longitudinal cognitive performance using PLS. This approach does not limit us to broad categorizations of decliners or maintainers, rather, we obtain continuous measures for each individual identifying the degree of expression of each of the identified brain-cognition patterns. The use of multimodal data and longitudinal cognitive measures is made possible by the unique dataset analysed. However, our study is limited by a smaller sample size in comparison to large scale neuroimaging analyses. It may be that more brain-cognition relationships would be identifiable in a larger sample. Our study also lacks an out of sample validation, as the unique longitudinal data makes a compatible out of sample dataset difficult to find. In addition to this, the Whitehall II Imaging Sub-study cohort contains a higher proportion of men compared to the general population and is relatively more educated. Thus, generalizability of our findings to the wider population is limited. While we were able to quantify 30-year cognitive trajectories, MRI data is currently available at a single time-point which limits investigations of longitudinal

brain-cognition relationships. Furthermore, while a combination of structural and diffusion MRI was used to provide a more comprehensive assessment of cortical microstructure, the limitations of MRI, in particular its resolution in comparison to the neural substrates under study, preclude us from inferring the cellular mechanisms which may be at play (65).

4.0 Conclusion

This work provides new information on brain-cognition relationships in a healthy elderly population. We uncover complex brain-cognition relationships using an unbiased data-driven approach, free of a priori definitions of cognitive maintainers or decliners and including a rich and comprehensive longitudinal cognitive data and multimodal MRI measures. This supports future works including multimodal data as well as cognitive trajectories to capture the full range of brain-cognition relationships. We also find the largest determinant of late life cognition is mid life cognition, as opposed to the rate of decline over time. This, and the associated link with widespread surface area measurements, support early and mid-life preventative measures of cognitive decline.

5.0 Methods

5.1 Sample

We used data from the Whitehall II Imaging Sub-Study (34), a random sample of 800 individuals from the Whitehall II Study of British civil servants, of which 775 received an MRI scan (33). These individuals have been assessed longitudinally since 1985 across a total of 12 waves thus far. Cognitive performance was assessed at 5 timepoints at University College London: Wave 5 (1997-1999), Wave 7 (2002-2004), Wave 9 (2007-2009), Wave 11 (2012-2013), and Wave 12 (2015-2016). Structural and diffusion weighted magnetic resonance imaging (MRI) was conducted at the University of Oxford between 2012-2016 (Figure 1). Participant inclusion criteria and sample selection are presented in the SI Methods.

5.2 MRI Acquisition

MRI data was acquired on one of two scanners - a 3T Siemens Magnetom Verio (Erlangen, Germany) (n=552) or a 3T Siemens Magnetom Prisma scanner (Erlangen, Germany) (n=223) at the FMRIB Centre in the Wellcome Centre for Integrative Neuroimaging (WIN), Oxford. T1 weighted images were acquired using a Multi-Echo MPRAGE (MEMPR) sequence ($1mm^3$, TR = 2530ms, TE = 1.79/3.65/5.51/7.37ms) on the Verio scanner and a closely-matched MPRAGE sequence on the Prisma scanner (1mm3, TR=1900ms, TE=3.97ms). Diffusion weighted imaging (DWI) was acquired with an identical sequence across both scanners, using monopolar diffusion encoding gradients with parallel imaging at 2mm isotropic (60 directions, $b=1500s/mm^2$). Detailed acquisition descriptions have been described elsewhere (34).

5.3 Obtaining Brain Microstructural Metrics

T1w images were preprocessed using the minc-bpipe-library (https://github.com/CoBrALab/minc-bpipe-library), including bias field correction, adaptive non-local means denoising (66), head masking and brain extraction (67) The resulting bias field corrected, head-masked images and brain masks of each subject were input into the CIVET algorithm (37, 38) (version 2.1.0) in order to obtain cortical mid-surfaces and vertex wise measures of cortical thickness (CT) and surface area (SA), describing CT and SA estimates at a total of 81924 points across the cortical mid-surface. Vertex wise CT and SA were blurred using 30 mm and 40 mm geodesic surface kernel, respectively. We masked out 4802 vertices located along the left and right midline as CT and SA estimates in this region are unreliable or nonexistent, resulting in a total of 77122 vertices valid for analysis. CIVET outputs were quality controlled for registration quality, grey/white matter classification accuracy, and surface abnormalities by RP.

DWI data were preprocessed using the FMRIB's diffusion toolbox (FDT), with a generative model approach to estimate and correct for distortions due to susceptibility, eddy currents, and head motion simultaneously. DTIFit (https://fsl.fmrib.ox.ac.uk/fsl/fslwiki/FDT) was used to generate maps of mean diffusivity (MD), fractional anisotropy (FA), and radial diffusivity (RD) for each subject. For each subject, MD, FA, and RD images were registered to their T1w image using a multispectral affine registration. The resulting transformations were used to transform the cortical mid-surface to the DWI space. Vertex wise samples of each of MD, FA, and RD were obtained using the transformed surfaces to correspond with the previously obtained vertex wise CT and SA measures. Like CT and SA data, left and right midline data was masked out resulting in a total of 77122 data points for each of MD, FA, and RD.

5.4 Identifying Components using Non-negative Matrix Factorization

We used non-negative matrix factorization (NMF) to identify microstructural components. NMF is a matrix approximation decomposition technique which decomposes an input matrix into two matrices describing components and weights. As the name suggests, NMF requires non negativity in both inputs and outputs, leading to an additive parts-based representation (25). Given an input matrix of dimensions m x n, NMF outputs a component matrix W (m x k), and a weight matrix H (k x n). The number of components, k, is defined by the user.

In this implementation, NMF input matrix is constructed by stacking the vertex x subject matrices of each microstructural metric together, forming a matrix with 77122 rows and 1990 columns (77122 vertices, 398 subjects * 5 metrics = 1990 columns). At each vertex, and for each microstructural metric, we model out the effect of scanner using linear regression and then perform z-scoring on the residuals. This minimizes any local scanner bias, and spatially normalizes each measure. The resulting residualized and z-scored matrices are then stacked side by side to form a matrix containing z-scored and residualized data across all microstructural metrics. This matrix is shifted by it's minimum value to create a non-negative input matrix for NMF. We used sklearn (version 0.23.1) to implement NMF with a non-negative singular

value decomposition initialization to improve sparsity (68). Granularity was selected through a split half stability analysis and a balance of spatial stability and model reconstruction accuracy (24).

5.5 Cognitive Function Trajectories

We used a total of 5 tests to measure cognitive performance. These include semantic fluency (in one minute, recall as many animals as possible), lexical fluency (in one minute, recall as many words starting with "S" as possible), short term memory (20 word free recall, recall within two minutes), inductive reasoning through the Alice-Heim 4-I (AH4) test (69), and vocabulary using the Mill Hill test (70, 71). We included the total AH4 score (inductive reasoning) as well as mathematical and verbal reasoning sub scores. For each test, a linear mixed effects model was performed with an interaction of baseline age and time since baseline as a fixed effect, a random slope of time since baseline, and random intercept for each subject (1).

$$TestScore \sim Baseline\ Age * Time + (1 + Time|Subject) \quad (1)$$

Models were implemented in R (version 3.6.3) using the nlme (version 3.1-149) package and implemented continuous autoregressive moving-average correlation structure to consider correlations between repeated measures on the same individual. Importantly, cognitive test data prior to the MRI time point (Wave 5-11 but excluding Wave 12) was included in the linear mixed effects modelling. For each model we extracted subject-specific intercepts and slopes (using the R coef() function), describing estimated performance in midlife as well as magnitude of decline over time. Wave 12 cognitive performance in each test except for the Mill Hill vocabulary test (not acquired at Wave 12) was then assessed as a function of the obtained brain-behavior patterns.

5.6 Partial Least Squares

To investigate microstructural cognition relationships, we performed a brain-behavior partial least squares analysis (PLS). PLS is a multivariate technique which aims to maximize the covariance between two sets of variables (35, 36, 39). In this implementation, brain variables correspond to a 398 x 50 matrix containing weightings of each subject within each of 10 components, for each of 5 microstructure metrics. behavioral data corresponds to a 398 X 14 matrix containing intercept and slope measures for each subject, for each of the 7 cognitive tests. PLS outputs latent variables (LV), each describing a pattern of covariance between microstructural NMF weights and cognitive intercepts and slopes. Each LV includes a singular value used to compute the proportion of total covariance explained, and statistical significance is assessed through permutation testing (n=10000). Bootstrap resampling is used to assess the contribution of each variable to a given LV (35, 39, 72, 73).

Acknowledgements

This research was funded in whole, or in part, by the Wellcome Trust [Grant number 203139/Z/16/Z]. For the purpose of open access, the author has applied a CC BY public copyright licence to any Author Accepted Manuscript version arising from this submission.

We would like to thank all contributors to the Whitehall II study. We thank all the participating civil service departments; the British Occupational Health and Safety Agency; the British Council of Civil Service Unions; all participating civil servants in the Whitehall II Study; and all members of the Whitehall II Study team at University College London who so helpfully collaborated with us. The Whitehall II Study team comprises research scientists, statisticians, study coordinators, nurses, data managers, administrative assistants, and data entry staff, who make the study possible. We would like to thank staff at the Wellcome Centre for Integrative Neuroimaging in Oxford who acquired scans, in particular Dr Nicola Filippini (DPhil) and research radiographers Michael Sanders, MSc, Jon Campbell, MMRTech, BcAppSc, Caroline Young, DCR(R), David Parker, BSc(Hons). Martin R. Turner, MA, MBBS, PhD, FRCP (Wellcome Centre for Integrative Neuroimaging, Oxford, United Kingdom), and his colleagues advised on incidental findings and taking over clinical responsibility for such participants.

The Whitehall II study is supported by the British Heart Foundation (RG/16/11/32334), UK Medical Research Council (K013351) and US National Institute on Aging (R01AG056477; RF1AG062553). The Whitehall II Imaging Sub-study was supported by the UK Medical Research Council (MRC) grants "Predicting MRI abnormalities with longitudinal data of the Whitehall II Sub-study" (G1001354; PI KPE; ClinicalTrials.gov Identifier: NCT03335696), and "Adult Determinants of Late Life Depression, Cognitive Decline and Physical Functioning - The Whitehall II Ageing Study" (MR/K013351/1; PI: MK). Working on this study was also supported by European Commission (Horizon 2020 grant "Lifebrain", 732592; co-PI KPE), the HDH Wills 1965 Charitable Trust (1117747; PI KPE) and the UK National Institute of Health Research (NIHR) Oxford Health Biomedical Research Centre (BRC). The Wellcome Centre for Integrative Neuroimaging (WIN) is supported by core funding from the Wellcome Trust (203139/Z/16/Z). **RP** is funded through the Fonds de Recherche du Quebec - Santé (Doctoral Training). **SS** is funded through Alzheimer's Society Research Fellowship (Grant Number 441), **KPE** through UK Medical Research Council (G1001354, MR/K013351/), HDH Wills 1965 Charitable Trust (1117747), Alzheimer Research UK (PPG2012A-5) and the European Commission (Horizon 2020 grant "Lifebrain", 732592), **EZs** UK Medical Research Council (G1001354, MR/K013351/), HDH Wills 1965 Charitable Trust (1117747), Horizon 2020 grant "Lifebrain", 732592; co-PI KPE), **MK** through UK MRC (MR/K013351/1, MR/R024227/1, MR/S011676/1), National Institute on Aging (NIH), US (R01AG056477), NordForsk (75021), Academy of Finland (311492), Helsinki Institute of Life Science Fellowship (H970), **ASM** through NIH (R01AG056477, R01AG062553).

Work on this study received institutional support from the UK National Institute of Health Research (NIHR) Oxford Health Biomedical Research Centre (BRC) and the Wellcome Centre for Integrative Neuroimaging (WIN). The WIN is supported by core funding from the Wellcome Trust (203139/Z/16/Z).

The views expressed are those of the authors and not necessarily those of the NHS, the NIHR or the Department of Health.

References

1. T. Salthouse, Selective review of cognitive aging. *Journal of International Neuropsychology* **16**, 754–760 (2010).

2. E. M. Tucker-Drob, Neurocognitive functions and everyday functions change together in old age. *Neuropsychology* **25**, 368–377 (2011).

3. R. S. Wilson, *et al.*, Individual differences in rates of change in cognitive abilities of older persons. *Psychol. Aging* **17**, 179–193 (2002).

4. E. M. Tucker-Drob, T. A. Salthouse, "Individual Differences in Cognitive Aging" in *The Wiley-Blackwell Handbook of Individual Differences*, T. Chamorro-Premuzic, S. von Stumm, A. Furnham, Eds. (Wiley-Blackwell, 2011), pp. 242–267.

5. S. Pudas, *et al.*, Brain characteristics of individuals resisting age-related cognitive decline over two decades. *J. Neurosci.* **33**, 8668–8677 (2013).

6. E. M. Tucker-Drob, Global and domain-specific changes in cognition throughout adulthood. *Dev. Psychol.* **47**, 331–343 (2011).

7. C. L. Tardif, *et al.*, Advanced MRI techniques to improve our understanding of experience-induced neuroplasticity. *Neuroimage* **131**, 55–72 (2016).

8. J. P. Lerch, *et al.*, Studying neuroanatomy using MRI. *Nat. Neurosci.* **20**, 314–326 (2017).

9. A. M. Hedman, N. E. M. van Haren, H. G. Schnack, R. S. Kahn, H. E. Hulshoff Pol, Human brain changes across the life span: a review of 56 longitudinal magnetic resonance imaging studies. *Hum. Brain Mapp.* **33**, 1987–2002 (2012).

10. A. M. Fjell, *et al.*, What is normal in normal aging? Effects of aging, amyloid and Alzheimer's disease on the cerebral cortex and the hippocampus. *Prog. Neurobiol.* **117**, 20–40 (2014).

11. M. E. Shaw, P. S. Sachdev, K. J. Anstey, N. Cherbuin, Age-related cortical thinning in cognitively healthy individuals in their 60s: the PATH Through Life study. *Neurobiol. Aging* **39**, 202–209 (2016).

12. A. J. Lowe, *et al.*, Targeting age-related differences in brain and cognition with multimodal imaging and connectome topography profiling. *Hum. Brain Mapp.* **40**, 5213–5230 (2019).

13. L. Marner, J. R. Nyengaard, Y. Tang, B. Pakkenberg, Marked loss of myelinated nerve fibers in the human brain with age. *J. Comp. Neurol.* **462**, 144–152 (2003).

14. G. Bartzokis, Age-related myelin breakdown: a developmental model of cognitive decline and Alzheimer's disease. *Neurobiol. Aging* **25**, 5–18 (2004).

15. C. Lebel, *et al.*, Diffusion tensor imaging of white matter tract evolution over the lifespan. *Neuroimage* **60**, 340–352 (2012).

16. Y. Stern, *et al.*, Whitepaper: Defining and investigating cognitive reserve, brain reserve, and brain maintenance. *Alzheimer's & Dementia* **16**, 1305–1311 (2020).

17. N. Raz, K. M. Rodrigue, Differential aging of the brain: Patterns, cognitive correlates and modifiers. *Neurosci. Biobehav. Rev.* **30**, 730–748 (2006).

18. A. L. C. Schneider, *et al.*, Neural correlates of domain-specific cognitive decline: The ARIC-NCS Study. *Neurology* **92**, e1051–e1063 (2019).

19. N. Philippi, *et al.*, Exploring anterograde memory: a volumetric MRI study in patients with mild cognitive impairment. *Alzheimers. Res. Ther.* **8**, 26 (2016).

20. E. T. Reas, *et al.*, Microstructural brain changes track cognitive decline in mild cognitive impairment. *Neuroimage Clin* **20**, 883–891 (2018).

21. M. F. Glasser, *et al.*, A multi-modal parcellation of human cerebral cortex. *Nature* **536**, 171–178 (2016).

22. J. Seidlitz, *et al.*, Morphometric Similarity Networks Detect Microscale Cortical Organization and Predict Inter-Individual Cognitive Variation. *Neuron* **97**, 231–247.e7 (2018).

23. A. R. Groves, *et al.*, Benefits of multi-modal fusion analysis on a large-scale dataset: life-span patterns of inter-subject variability in cortical morphometry and white matter microstructure. *Neuroimage* **63**, 365–380 (2012).

24. R. Patel, *et al.*, Investigating microstructural variation in the human hippocampus using non-negative matrix factorization. *Neuroimage* **207**, 116348 (2020).

25. D. D. Lee, H. S. Seung, Learning the parts of objects by non-negative matrix factorization. *Nature* **401**, 788–791 (1999).

26. A. Sotiras, S. M. Resnick, C. Davatzikos, Finding imaging patterns of structural covariance via Non-Negative Matrix Factorization. *Neuroimage* **108**, 1–16 (2015).

27. J. Persson, *et al.*, Structure-function correlates of cognitive decline in aging. *Cereb. Cortex* **16**, 907–915 (2006).

28. M. Josefsson, X. de Luna, S. Pudas, L.-G. Nilsson, L. Nyberg, Genetic and lifestyle predictors of 15-year longitudinal change in episodic memory. *J. Am. Geriatr. Soc.* **60**, 2308–2312 (2012).

29. J. Persson, *et al.*, Longitudinal structure-function correlates in elderly reveal MTL dysfunction with cognitive decline. *Cereb. Cortex* **22**, 2297–2304 (2012).

30. D. C. Park, P. Reuter-Lorenz, The Adaptive Brain: Aging and Neurocognitive Scaffolding. *Annu. Rev. Psychol.* **60**, 173–196 (2009).

31. M. Rönnlund, L. Nyberg, L. Bäckman, L.-G. Nilsson, Stability, growth, and decline in adult life span development of declarative memory: cross-sectional and longitudinal data from a population-based study. *Psychol. Aging* **20**, 3–18 (2005).

32. J. O. Goh, Y. An, S. M. Resnick, Differential trajectories of age-related changes in components of

executive and memory processes. *Psychol. Aging* **27**, 707–719 (2012).

33. M. Marmot, E. Brunner, Cohort Profile: the Whitehall II study. *Int. J. Epidemiol.* **34**, 251–256 (2005).

34. N. Filippini, *et al.*, Study protocol: The Whitehall II imaging sub-study. *BMC Psychiatry* **14**, 159 (2014).

35. A. R. McIntosh, N. J. Lobaugh, Partial least squares analysis of neuroimaging data: applications and advances. *Neuroimage* **23 Suppl 1**, S250–63 (2004).

36. A. R. McIntosh, B. Mišić, Multivariate statistical analyses for neuroimaging data. *Annu. Rev. Psychol.* **64**, 499–525 (2013).

37. Y. Ad-Dab'bagh, *et al.*, The CIVET image-processing environment: a fully automated comprehensive pipeline for anatomical neuroimaging research in *Proceedings of the 12th Annual Meeting of the Organization for Human Brain Mapping*, (Florence, Italy, 2006).

38. J. P. Lerch, A. C. Evans, Cortical thickness analysis examined through power analysis and a population simulation. *Neuroimage* **24**, 163–173 (2005).

39. A. Krishnan, L. J. Williams, A. R. McIntosh, H. Abdi, Partial Least Squares (PLS) methods for neuroimaging: a tutorial and review. *Neuroimage* **56**, 455–475 (2011).

40. M. M. Esiri, Ageing and the brain. *J. Pathol.* **211**, 181–187 (2007).

41. N. A. Goriounova, *et al.*, Large and fast human pyramidal neurons associate with intelligence. *Elife* **7** (2018).

42. D. Vidal-Pineiro, *et al.*, Cellular correlates of cortical thinning throughout the lifespan. *Sci. Rep.* **10**, 21803 (2020).

43. Y. Patel, *et al.*, Virtual histology of cortical thickness and shared neurobiology in 6 psychiatric disorders. *JAMA Psychiatry* **78**, 47–63 (2021).

44. C. Beaulieu, The basis of anisotropic water diffusion in the nervous system--a technical review. *NMR Biomed.* **15**, 435–455 (2002).

45. D. J. Madden, *et al.*, Diffusion tensor imaging of cerebral white matter integrity in cognitive aging. *Biochim. Biophys. Acta* **1822**, 386–400 (2012).

46. B. Benedetti, *et al.*, Influence of aging on brain gray and white matter changes assessed by conventional, MT, and DT MRI. *Neurology* **66**, 535–539 (2006).

47. J. A. Chad, O. Pasternak, D. H. Salat, J. J. Chen, Re-examining age-related differences in white matter microstructure with free-water corrected diffusion tensor imaging. *Neurobiol. Aging* **71**, 161–170 (2018).

48. U. I. Tuor, *et al.*, Cellular correlates of longitudinal diffusion tensor imaging of axonal degeneration following hypoxic-ischemic cerebral infarction in neonatal rats. *Neuroimage Clin* **6**, 32–42 (2014).

49. S.-K. Song, *et al.*, Dysmyelination revealed through MRI as increased radial (but unchanged axial) diffusion of water. *Neuroimage* **17**, 1429–1436 (2002).

50. S.-W. Sun, H.-F. Liang, A. H. Cross, S.-K. Song, Evolving Wallerian degeneration after transient retinal ischemia in mice characterized by diffusion tensor imaging. *Neuroimage* **40**, 1–10 (2008).

51. S.-K. Song, J. H. Kim, S.-J. Lin, R. P. Brendza, D. M. Holtzman, Diffusion tensor imaging detects age-dependent white matter changes in a transgenic mouse model with amyloid deposition. *Neurobiol. Dis.* **15**, 640–647 (2004).

52. A. L. Alexander, J. E. Lee, M. Lazar, A. S. Field, Diffusion tensor imaging of the brain. *Neurotherapeutics* **4**, 316–329 (2007).

53. R. J. Zatorre, R. D. Fields, H. Johansen-Berg, Plasticity in gray and white: neuroimaging changes in brain structure during learning. *Nat. Neurosci.* **15**, 528–536 (2012).

54. Y. Assaf, O. Pasternak, Diffusion tensor imaging (DTI)-based white matter mapping in brain research: a review. *J. Mol. Neurosci.* **34**, 51–61 (2008).

55. M. Ewers, Reserve in Alzheimer's disease: update on the concept, functional mechanisms and sex differences. *Curr. Opin. Psychiatry* **33**, 178–184 (2020).

56. A. Soldan, C. Pettigrew, M. Albert, Cognitive Reserve from the Perspective of Preclinical Alzheimer Disease: 2020 Update. *Clin. Geriatr. Med.* **36**, 247–263 (2020).

57. S. Gregory, *et al.*, Operationalizing compensation over time in neurodegenerative disease. *Brain* **140**, 1158–1165 (2017).

58. P. Rakic, Specification of cerebral cortical areas. *Science* **241**, 170–176 (1988).

59. P. Rakic, Radial unit hypothesis of neocortical expansion. *Novartis Found. Symp.* **228**, 30–42; discussion 42–52 (2000).

60. A. B. Storsve, *et al.*, Differential longitudinal changes in cortical thickness, surface area and volume across the adult life span: regions of accelerating and decelerating change. *J. Neurosci.* **34**, 8488–8498 (2014).

61. M. S. Panizzon, *et al.*, Distinct genetic influences on cortical surface area and cortical thickness. *Cereb. Cortex* **19**, 2728–2735 (2009).

62. S. R. Cox, *et al.*, Brain cortical characteristics of lifetime cognitive ageing. *Brain Struct. Funct.* **223**, 509–518 (2018).

63. K. B. Walhovd, *et al.*, Neurodevelopmental origins of lifespan changes in brain and cognition. *Proc. Natl. Acad. Sci. U. S. A.* **113**, 9357–9362 (2016).

64. S. Suri, *et al.*, Association of Midlife Cardiovascular Risk Profiles With Cerebral Perfusion at Older Ages. *JAMA Netw Open* **2**, e195776 (2019).

65. C. L. Tardif, *et al.*, Investigation of the confounding effects of vasculature and metabolism on

computational anatomy studies. *Neuroimage* **149**, 233–243 (2017).

66. J. V. Manjón, P. Coupé, L. Martí-Bonmatí, D. L. Collins, M. Robles, Adaptive non-local means denoising of MR images with spatially varying noise levels. *J. Magn. Reson. Imaging* **31**, 192–203 (2010).

67. S. F. Eskildsen, *et al.*, BEaST: brain extraction based on nonlocal segmentation technique. *Neuroimage* **59**, 2362–2373 (2012).

68. C. Boutsidis, E. Gallopoulos, SVD based initialization: A head start for nonnegative matrix factorization. *Pattern Recognit.* **41**, 1350–1362 (2008).

69. A. W. Heim, Manual for the AH4 group test of general intelligence. *Windsor: NFER* (1970).

70. J. C. Raven, Guide to using the Mill Hill Vocabulary Scale with the Progressive Matrices Scales. **64** (1958).

71. A. Singh-Manoux, *et al.*, Timing of onset of cognitive decline: results from Whitehall II prospective cohort study. *BMJ* **344**, d7622 (2012).

72. K. Nordin, *et al.*, Structural whole-brain covariance of the anterior and posterior hippocampus: Associations with age and memory. *Hippocampus* **28**, 151–163 (2018).

73. Y. Zeighami, *et al.*, A clinical-anatomical signature of Parkinson's disease identified with partial least squares and magnetic resonance imaging. *Neuroimage* (2017) https:/doi.org/10.1016/j.neuroimage.2017.12.050.